aerospace

MDPI

Article

Dynamic Analysis of the Rod-Traction System for Ship-Borne Aircraft Under High Sea States

Guofang Nan *, Chen Zhang, Bodong Zhang, Sirui Yang and Jinrui Hu

School of Energy and Power Engineering, University of Shanghai for Science and Technology, Shanghai 200093, China; 243420293@st.usst.edu.cn (C.Z.); 243420245@st.usst.edu.cn (B.Z.); 223370219@st.usst.edu.cn (S.Y.); 242230056@st.usst.edu.cn (J.H.)

* Correspondence: ngf@usst.edu.cn

Abstract

The transfer of aircraft on deck relies on the traction system, which is easily affected by the offshore environment. Violent ship motion in the complex marine environment poses a great threat to the aircraft traction process, such as the tire sideslip, off-ground phenomena, the aircraft overturning, traction rod fatigue fracture, and so on. Therefore, it has merits in both academia and engineering practice to study the dynamic behaviors of the ship-borne aircraft towing system under high sea states. Considering the intricate coupling motions of the hull roll, pitch, and heave, the dynamic analysis of the towing system with rod are carried out based on the multibody dynamics theory. The influence of the sea state level and the traction speed on the dynamic characteristics of the towing system is investigated. The results indicate that noticeable tire sideslip occurs under sea state 3, with the peak lateral tire force increasing by approximately 250% compared with sea state 2. Under sea state 4, intermittent off-ground phenomena are observed, accompanied by a further increase of about 22% in lateral tire force. These findings provide quantitative insights into the dynamic characteristics and operational limits of rod-traction systems for ship-borne aircraft in rough marine environments.

Keywords: ship-borne aircraft; rod-traction; high sea states; ship motions; traction force; multibody dynamics; carrier deck operations; tire–deck interaction

1. Introduction

The transfer of ship-borne aircraft by tractor under the complex maritime states has multiple advantages. Research on rod towing for ship-borne aircraft in complicated environments is crucial for ensuring the safety and stability of the towing process of the aircraft. When the aircraft lands on a ship deck, the limited space on the deck requires high stability and precision in rough seas. With their inherent advantages of high flexibility, strong stability, and the absence of auxiliary equipment on deck, tractors effectively meet the requirements for aircraft movement and positioning on ship decks. Therefore, this paper mainly studies the traction dynamic characteristics of ship-borne aircraft under high sea states and provides a safety reference for the traction operation of ship-borne aircraft.

Considerable research efforts have been devoted to the dynamic modeling and control of ship-borne aircraft systems. Wang X. W. et al. [1] introduced a computationally efficient hierarchical seeding scheme combined with model predictive tracking for coordinated deck taxiing. Leveille [2] employed the Shipboard-Spatial Motion and Securing Helicopter (SSMASH) method to investigate helicopter–ship coupled dynamics, while Vilchis et al. [3] developed

Check for updates

Academic Editor: Konstantinos Kontis

Received: 24 November 2025
Revised: 16 January 2026
Accepted: 21 January 2026
Published: 22 January 2026

Copyright: © 2026 by the authors. Licensee MDPI, Basel, Switzerland. This article is an open access article distributed under the terms and conditions of the Creative Commons Attribution (CC BY) license.

nonlinear helicopter models and corresponding control strategies. Li Y. J. et al. [4] proposed a six-degree-of-freedom Iterative Dynamic Re-weighting Algorithm (IDRA) to improve aircraft modeling efficiency.

From a multibody dynamics perspective, Yang H. et al. [5] established a Lagrange-based kinetic model for an aircraft–tractor system, and Zhao D. X. et al. [6] constructed a multibody dynamics model to analyze aircraft towing forces. Fricke et al. [7], York et al. [8], Linn et al. [9,10], and Cui et al. [11] focused on landing gear–tire–ground interaction modeling and dynamic response analysis, providing important foundations for ground operation dynamics. Lu X et al. [12] developed the tractor–aircraft system model through Adams software, and the study found that the binding force at both ends of the front landing gear can reduce the acceleration offset between the tractor and the aircraft during braking.

The vulnerability of ship-borne aircraft to wave-induced ship motions has also attracted increasing attention. Dooley et al. [13] investigated the effects of waves and ship motions on airwake characteristics and helicopter operations, while Shukla [14] provided a comprehensive review of ship–helicopter coupled airwake interactions. Memon et al. [15] developed a motion-cueing optimization method for flight simulators to study shipboard helicopter landings under varying wind and wave conditions, improving the realism and safety of simulated training. Zhu et al. [16] analyzed ship resonance phenomena through simulation experiments and verified their effects on shipboard aircraft operations, showing that resonance-induced amplification of ship motions can adversely affect deck operation safety. Wen Z. et al. [17] developed a six-degree-of-freedom ship motion model to study aircraft attitude evolution during deck operations. Furthermore, Byeong-Woo Yoo et al. [18] established a dynamic simulation model incorporating ship motions and landing gear–deck interactions to analyze aircraft movement characteristics and deck operation stability.

In recent years, research has expanded toward autonomous dispatch, path planning, and control strategies for carrier deck operations. Liu J. et al. [19] reformulated the bar-free towed shipboard aircraft as a tractor–trailer system and proposed an efficient offline trajectory planning algorithm. Zhang Z. L. et al. [20] developed a genetic collision avoidance algorithm with kinematic constraints to generate optimal sliding paths for irregular targets in complex obstacle environments, satisfying radius-of-gyration limitations. Under highly constrained deck environments, Li et al. [21] introduced an iterative Safe Dispatch Corridor (iSDC) framework that integrates Kinematics-Informed Bidirectional RRT* (KIB-RRT*) planning with corridor optimization, significantly improving dispatch efficiency. From a control perspective, Wang and Yu [22] investigated the stability of carrier-based aircraft tractors using an adaptive sliding mode control method based on radial basis function (RBF) neural networks. Sun et al. [23] further combined Closed-Loop RRT (CL-RRT) with Model Predictive Control (MPC) to enhance path feasibility and tracking performance for aircraft towing systems.

Domestic and international scholars have conducted extensive research on key technologies such as carrier-based aircraft multibody dynamics, tire loads, arresting systems, trajectory planning, and towing systems, achieving significant progress. However, existing studies mostly focus on relatively stable deck environments. The mechanisms by which complex coupled dynamics of the aircraft–tow bar–towing vehicle system affect towing safety and component loads under ship motion in severe sea conditions remain insufficiently explored. Therefore, this study aims to establish a dynamic model that accounts for the coupling between ship multi-degree-of-freedom motion and the towing system under high sea states, with a focus on analyzing the dynamic response and critical component loads of carrier-based aircraft towing in typical severe sea conditions, in order to provide quantitative evidence and theoretical support for safe towing operations under complex sea states.

The main contribution of this study lies in the establishment of a unified full-system dynamic model for ship-borne aircraft rod-traction operations under high sea states. Unlike

existing studies that focus on isolated subsystems or quasi-static deck assumptions, the proposed framework integrates ship motion excitation, tow rod dynamics, tire–deck interaction, and traction speed control into a single multibody dynamic model, providing a system-level perspective on towing stability in severe marine environments. It should be emphasized that this study does not aim to propose a new fundamental dynamics theory or predictive model. Instead, its contribution lies in providing an engineering-oriented, system-level quantitative analysis of the coupled aircraft–tow rod–tractor–ship dynamics under high sea states, which are insufficiently addressed in the existing literature.

2. Modeling and Methodology of the Ship-Borne Aircraft Rod-Traction System

2.1. Methods and Software

The modeling framework presented in this section is formulated in a general form and is applicable to a wide range of ship-borne aircraft rod-traction systems. Specific system parameters are introduced later only for numerical case studies.

A time-domain multibody dynamics approach is adopted to investigate the towing behavior of ship-borne aircraft under high sea states. The aircraft, tow rod, tractor, landing gears, tires, and ship deck are modeled as a coupled dynamic system. Rigid-body assumptions are applied to the aircraft fuselage, tractor body, and tow rod, while elastic-damping elements are used to represent landing gear struts, tire–deck contact, and tow rod deformation. It should be emphasized that the significance of the proposed model lies not in the individual dynamic formulations but in the explicit coupling of multiple subsystems that are usually treated independently in existing studies. The multibody dynamics approach adopted in this study is an engineering-oriented formulation rather than a fully generalized multibody dynamics framework. The system consists of multiple rigid bodies and simplified flexible components, whose dynamics are described using Newton–Euler equations and coupled through force interactions and coordinate transformations. This approach is suitable for analyzing system-level dynamic responses of complex engineering systems while maintaining computational efficiency.

Ship motions are prescribed as harmonic roll, pitch, and heave excitations with amplitudes and periods determined by sea state levels reported in the literature. Wind loads acting on the aircraft and tractor are applied at their centers of gravity based on aerodynamic drag formulations.

MATLAB R2021b was employed as the primary simulation platform for this study. The coupled multibody dynamic model of the aircraft–tow bar–tractor–ship system was implemented using custom MATLAB scripts. Time-domain simulations were performed to solve the governing equations of motion under different sea state conditions. In addition, a Proportional–Integral–Derivative (PID) controller was implemented within the MATLAB environment to regulate the tractor traction speed. All dynamic response analyses, including traction forces and tire loads, were carried out based on the simulation results.

2.2. System Geometry and Boundary Conditions

The towing system consists of the aircraft, landing gears, tires, tow rod, tractor, and ship deck. The aircraft is connected to the tractor through a rigid tow rod via hinge joints, allowing force transmission while constraining relative motion. The tires maintain continuous contact with the deck through elastic-damping elements, representing tire–deck interaction.

The ship deck motion is prescribed as a boundary excitation and is not solved dynamically. Roll, pitch, and heave motions are applied to the deck reference frame according to harmonic functions corresponding to different sea state levels. The tractor motion is controlled by a closed-loop speed controller, while the aircraft responds passively to traction- and deck-induced excitations.

3. Dynamic Modeling of Ship-Borne Aircraft Traction Under High Sea States

The main tow system of the ship-borne aircraft includes the aircraft, the tires, the tractor, the tow rods, and the ship. The tires are connected to the aircraft via the landing gear and contact with the deck. In rod-traction systems, the tractor and aircraft are linked through tow rods by hinge joints. Given that aircraft towing typically is at low speeds, the following modeling assumptions are made. (1) The fuselage of the aircraft and the tractor body are regarded as rigid bodies, and all mass is assumed to reside at the center of gravity. (2) The traction hinge is rigid connection. (3) The motion of the aircraft traction system is coupled with ship motion. At the beginning of the modeling process, it is hypothesized that increasing sea state severity will amplify traction rod forces and tire lateral forces due to coupled ship motions, thereby reducing towing stability. In addition, for straight-line towing under high sea states, appropriate increases in traction speed are expected to mitigate traction force fluctuations and improve system stability.

Although generalized coordinates and constraint equations are not explicitly defined, they are implicitly represented through the transformation relationships among the inertial, aircraft, tractor, and ship coordinate systems (Figure 1).

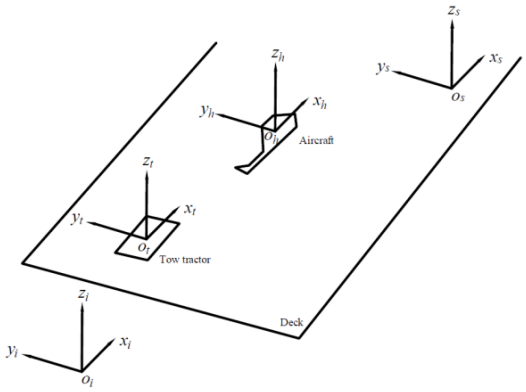


Figure 1. Overall coordinate schematic of the carrier-based aircraft tow system.

3.1. High Sea States and Ship Motion

3.1.1. High Sea States

For high sea states, there is no clear definition in form at present. Generally, sea states are classified according to wave type and wave height. Wave type and wave height are different under the different sea states. The higher the sea state level, the worse the sea environment, and the more complex the corresponding excitation. The wave characteristics corresponding to each sea state level are shown in Table 1. Since the research object of this paper is the traction system on the small deck, the traction system is more sensitive to the waves during traction operation. Therefore, the four-level sea state and above is regarded as a high sea state in this study.

Table 1. Wave characteristics corresponding to each sea state level.

Sea State Level	Name	Wave Height (m)	Sea Surface Characteristics
0	No wave	0	The sea is calm
1	Smooth sea	0~0.1	Tiny ripples of states appear
2	Wavelet	0.1~0.5	Waves are small, tiny ripples, shorter wavelengths, and wave crests do not break
3	Slight sea	0.5~1.25	The wave is not large, the peak is broken, and the waves appear

Table 1. *Cont.*

Sea State Level	Name	Wave Height (m)	Sea Surface Characteristics
4	Moderate sea	1.25~2.5	There are more wave peaks breaking, white waves appearing, and appearing in groups
5	Big wave	2.5~4.0	There are tall peaks, more foam peaks, and occasional droplets

3.1.2. Ship Motion

Considering that the traction system of ship-borne aircraft under high sea states encompasses the coupling motion of numerous components such as the aircraft, the tractor, and the vessel, it is essential to establish different coordinate systems to comprehensively calculate the transient dynamics of the whole multibody system. Four coordinate systems are defined in this paper, which are the inertial coordinate system ($o_i x_i y_i z_i$), the aircraft coordinate system ($o_h x_h y_h z_h$), the tractor coordinate system ($o_t x_t y_t z_t$), and the hull coordinate system ($o_s x_s y_s z_s$), as shown in Figure 1.

Ship-borne aircraft are susceptible to ship motion during the traction process, especially in high sea states. Waves caused by other factors such as sea winds act on the hull and cause intense ship motion. At the same time, the tires are directly in contact with the deck of the ship, so that the complex motion of the ship is directly fed back to the tractor-aircraft system, which undoubtedly threatens the traction process of ship-borne aircraft. Therefore, analyzing the ship's motion is essential before studying the traction dynamics of ship-borne aircraft. The general ship motion may be affected by various nonlinear irregular waves. In order to facilitate modeling, the hull is regarded as a rigid body in this paper. The hull generates six-degree-of-freedom (DOF) motion under the action of wind load and waves. The motion includes the roll, the pitch, the heave, the yaw, the surge, and the sway. Due to the relatively large influence of the rolling, pitching, and heaving on the motion of the hull, the motion in these three directions is selected as the research object. Figure 2 illustrates the schematic diagram of the specific ship motion where the rolling is the motion of the hull around the x-axis, the pitching is the motion of the hull around the y-axis, and heaving is the heave motion of the hull in the z-axis. The motion of a ship in an irregular wave is composed of the superposition of several regular waves with different frequencies and periods. In this paper, the motion of a ship is regarded as harmonic motion [20], and the specific motion form of the ship is as follows:

$$\begin{cases} \varphi = \varphi_0 \sin(2\pi t / T_\varphi + \eta_\varphi) \\ \theta = \theta_0 \sin(2\pi t / T_\theta + \eta_\theta) \\ z = z_0 \sin(2\pi t / T_z + \eta_z) \end{cases} \tag{1}$$

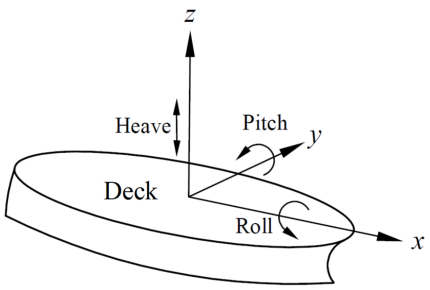


Figure 2. Schematic diagram of ship motion: the rolling is the motion of the hull around the x-axis, the pitching is the motion of the hull around the y-axis, and heaving is the heave motion of the hull in the z-axis.

3.2. Force Analysis for Traction System

To examine how traction systems evolve over time, the first step is to analyze the landing gear configuration, the wind load, the tow bar, and tractors' driving forces. The undercarriage is simplified in this paper, as demonstrated in Figure 3. The normal load on the undercarriage is determined by the following formula.

$$F_l = k_2\, d + c_2\, \dot{d} \tag{2}$$

where k_2 is the landing gear strut stiffness, c_2 is the damping constant, d is the pillar displacement, and $\dot{d}$ is the pillar speed.

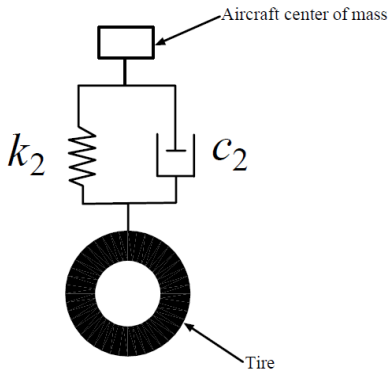


Figure 3. Telescopic landing gear diagram.

Tractors and aircraft are vulnerable to wind loads. In the study, it is assumed that air resistance is applied to the center of gravity for tractors and aircraft, and the airflow loading acting on tractors and aircraft is written as

$$F_{wh} = \frac{1}{2} \times C_{\mathrm{d}} \times S_h \times V^2 \tag{3}$$

$$F_{wt} = \frac{1}{2} \times C_{\mathrm{d}} \times S_t \times V^2 \tag{4}$$

where C_d is the wind resistance coefficient, S_h and S_t are the vertical projected areas of the aircraft and the tractor, respectively, $V = V_{wind} + V_{ship}$ is the synthetic wind speed, and the direction is the wind synthesis direction. The specific diagram is shown in Figure 4.

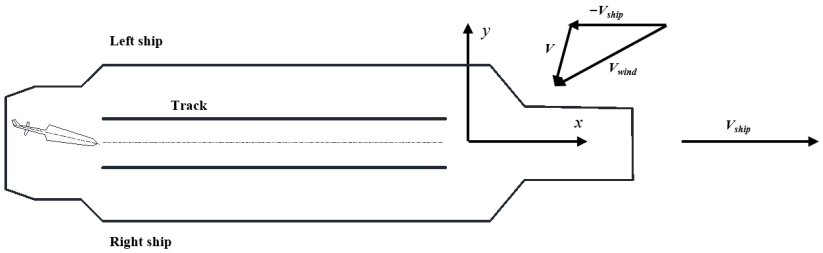


Figure 4. Schematic diagram of the speed synthesis.

For the traction with a towing rod, the two ends of the traction rod are connected to the aircraft and the tractor, respectively. The traction rod is subject to forces given by

$$F_g = k \times \Delta L + c \times \Delta \dot{L} \tag{5}$$

where k and c are the stiffness and damping of the traction rod, respectively, and ΔL is the stretch experienced by the traction rod. $\Delta \dot{L}$ is the deformation speed of the traction rod.

The tractor is mainly driven by the rear wheels whose driving force can be expressed as

$$F_q = F_g + F_{wt} \tag{6}$$

where F_g is the traction force that the aircraft needs to provide to the tractor, and F_{wt} is the resistance that the tractor is subjected to during driving, mainly including air resistance, acceleration resistance, wheel driving resistance, slope resistance, and the gravitational force component of the aircraft and tractor in their respective coordinate system.

3.3. Dynamics Modeling of Traction System with Rod

Figure 5 presents the force-analysis diagram of the rod-traction system. Constraints within the system are reflected by tire–deck contact models and force transmission between the aircraft, tow rod, and tractor (Figure 5). According to the constraints between the tractor, the traction rod, and the aircraft, the synthes external force and torque of the aircraft and the tractor are derived, respectively. The synthes external force of the aircraft fuselage under rod-traction is as follows:

$$\sum F_{ha} = F_{cha_i} + F_{g_i} + F_{wh_i} - F_{Gh_i} \tag{7}$$

where F_{cha_i} is the force of the tire on the aircraft in the inertial system, F_{g_i} is the force exerted on the aircraft by the tow rod, F_{wh_i} is the lateral air resistance of the aircraft, and F_{Gh_i} is the gravity of the aircraft in the inertial system. The external torque of the aircraft fuselage under the rod-traction is as follows:

$$\sum M_{ha} = M_{cha} + M_{gh} + M_{wh} \tag{8}$$

where M_{cha} is the torque of the tire to the aircraft, M_{gh} is the torque of the traction rod to the aircraft, and M_{wh} is the torque of the lateral air resistance to the aircraft. The synthes external force of the tractor is expressed as

$$\sum F_{ta} = F_{cta_i} - F_{g_i} + F_{wt_i} - F_{Gt_i} \tag{9}$$

where F_{cta_i} is the force of the tire on the tractor in the inertial system, F_{g_i} is the force exerted by the traction rod on the aircraft, F_{wt_i} is the lateral air resistance of the aircraft, and F_{Gt_i} is the gravity of the aircraft in the inertial system. The external torque of the tractor is written as

$$\sum M_{ta} = M_{cta} + M_{gt} + M_{wt} \tag{10}$$

where M_{cta} is the torque of the tire on the tractor, M_{gt} is the torque of the traction rod on the tractor, and M_{wt} is the torque of the lateral air resistance on the tractor.

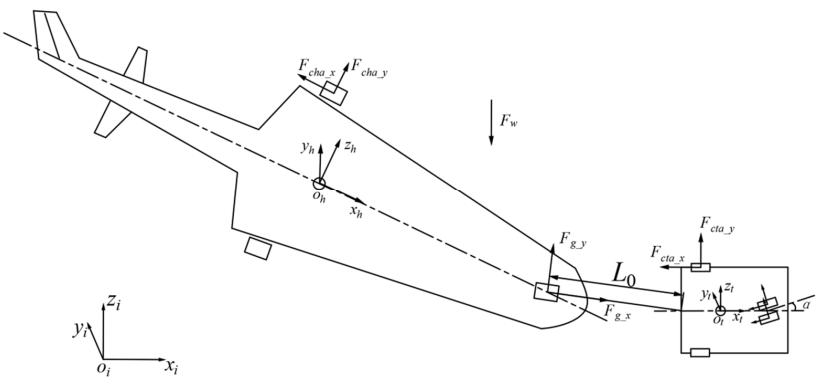


Figure 5. The schematic diagram of the rod-traction system of the ship-borne aircraft.

3.4. Proportional–Integral–Derivative Speed Control

The traction device built in this study can adjust the travel speed of the tractor with the help of the Proportional–Integral–Derivative (PID) algorithm. Fine-tuning the PID gains keeps the tractor's speed steady across varying field states. The formula of the PID control algorithm can be written as

$$u(t) = k_p e(t) + k_i \int_0^t e(t)dt + k_d \frac{de(t)}{dt} \tag{11}$$

where $u(t)$ is the output control quantity, which is the first derivative of the driving force of the tractor tire; k_p is the proportional amplification factor; k_i is the integral time constant; and k_d is a differential time constant. Figure 6 demonstrates the principle of controlling the speed of the tractor. Speed regulation proceeds in closed-loop cycles: a target value is fed in, the mismatch $e(t)$ with the current ground speed is measured, and a PID-generated correction $u(t)$ drives the propulsion system. The resulting new speed is immediately compared with the target to produce an updated error, and the sequence repeats until the tractor settles at the demanded velocity. Here, $e(t)$ denotes the instantaneous difference between commanded and measured travel speeds.

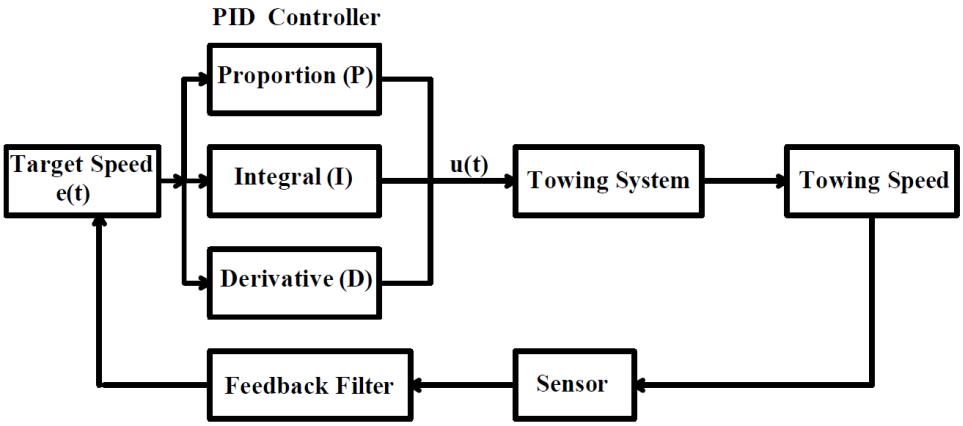


Figure 6. Principle diagram of PID speed control for traction system.

4. Dynamics Analysis of Rod-Traction System Under High Sea States

4.1. Parameter Sources and Justification

The parameters summarized in Tables 2–5 are derived from an existing engineering model of a ship-borne aircraft towing system rather than from publicly available commercial datasets. The aircraft parameters correspond to a representative three-point landing gear helicopter, and its mass properties, geometric dimensions, and moments of inertia are determined based on engineering design specifications.

Table 2. Related parameters for first three-point helicopter.

Parameter Names	Meaning of Parameters	Values
Mass of aircraft fuselage	Aircraft mass (kg)	13,000
Mass of aircraft tire	Aircraft tire mass (kg)	150
Centroid position of aircraft	Vertical distance from center of mass to deck (m)	2.8
	Horizontal distance from the center of mass to the main landing gear shaft (m)	2

Table 2. *Cont.*

Parameter Names	Meaning of Parameters	Values
Moment of inertia $I_{xx}/I_{yy}/I_{zz}$	Moment of inertia around the *X* axis (kg·m^2)	18,000
	Moment of inertia around *Y* axis(kg·m^2)	32,666.7
	Moment of inertia around *Z* axis (kg·m^2)	50,666.7
Distance of main landing gear	Horizontal distance between two main landing gears (m)	4
Distance between front landing gear and main landing gear	The horizontal distance between the front axle and the main axle (m)	6.6

Table 3. Parameters of landing gear.

Parameter Names	Meaning of Parameters	Values
Main landing gear	Stiffness (N/mm)	370.7
	Damping (N·s/mm)	49.9
Nose landing gear	Stiffness (N/mm)	884.4
	Damping (N·s/mm)	15.3

Table 4. Parameters of traction rod.

Parameter Names	Meaning of Parameters	Values
Stiffness	Longitudinal stiffness (N/mm)	4000
Damping	Longitudinal damping (N·s/mm)	60
Length	Longitudinal length of traction rod (mm)	4000

Table 5. Tractor parameters.

Parameter Names	Meaning of Parameters	Values
Tractor mass	Tractor mass (kg)	4000
Wheel mass	Tractor tire mass (kg)	150
Centroid position of tractor	Vertical distance from center of mass to deck (m)	0.128
	Horizontal distance from the center of mass to the main landing gear shaft (m)	2
$I_{xx}/I_{yy}/I_{zz}$ Moment of inertia	Moment of inertia around the *X* axis (kg·m^2)	3300
	Moment of inertia around *Y* axis (kg·m^2)	6900
	Moment of inertia around *Z* axis (kg·m^2)	3700
Distance between two front suspensions	Horizontal distance between two front suspensions (m)	2.9
Distance between two rear suspensions	Horizontal distance between two rear suspensions(m)	0.35
Distance between front suspension and rear suspension	Horizontal distance between front suspension and rear suspension axle (m)	2.37

The landing gear stiffness and damping coefficients are selected according to structural design data and typical values used in carrier-based aircraft dynamic analyses, ensuring realistic shock absorption and load transfer characteristics. The tow rod stiffness and damping parameters are determined based on engineering strength and fatigue requirements to reflect its load-bearing and vibration attenuation capabilities during towing operations.

The tractor parameters are obtained from a scaled engineering towing vehicle model, with mass distribution and geometric dimensions consistent with practical deck operation requirements. All parameters have been carefully checked to ensure physical consistency and realistic dynamic behavior of the coupled system.

It should be emphasized that the tire mass used in the model represents an equivalent dynamic mass of the wheel–landing gear assembly rather than the mass of a standalone commercial aircraft tire. The stiffness and damping parameters of the landing gear represent equivalent dynamic properties under carrier deck operating conditions and are not intended to correspond to nominal values obtained from standard ground-based tests.

4.2. Modeling Parameters

The research object of this paper is the first three-point helicopter. The front landing gear tire is the steering wheel, and the main landing gear wheel is fixed on the aircraft fuselage. Table 2 lists the helicopter's key parameters. Table 3 presents the landing gear parameters. Table 4 presents the specific parameters of the traction rod, and the pertinent parameters of the tractor are listed in Table 5.

The tractor selected in this paper is a scaled-down tele-operated trailer, and Table 5 presents its specific parameters.

4.3. Influence of Sea State Level on the Dynamics of Traction System

In this paper, the four-level sea states and above are taken as high sea states. According to the existing public literature, the roll, pitch and heave amplitudes and periods under 1 to 5 levels of sea states are listed, respectively, as shown in Table 6. The wind level and wind velocity range corresponding to each sea condition level are shown in Table 7.

Table 6. Parameters for sea state levels.

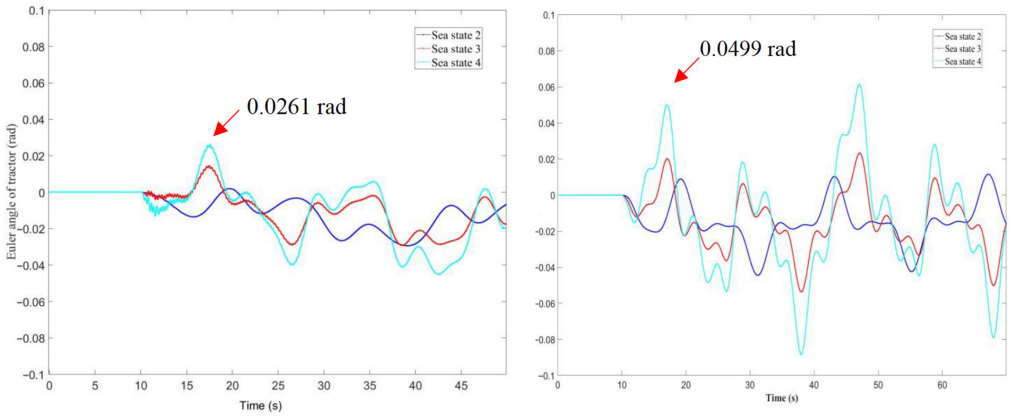
Sea State Level	1	2	3	4	5
φ_0 (°)	3.25	6.33	9.10	13.52	17.55
T_1 (s)	10	8	6	6	4
θ_0 (°)	1.15	2.10	3.25	4.09	5.05
T_2 (s)	14	12	10	10	8
Z_0 (m)	0.19	0.29	0.30	0.42	0.51
T_3 (s)	14	12	10	10	8

Table 7. Wind level and wind velocity range corresponding to sea state level.

Sea State Level	The Corresponding Wind Level	Wind Velocity (m/s)
0	0 level	0.0~0.2
1	1~2 level	0.3~3.3
2	2~4 level	1.6~7.9
3	4~5 level	5.5~10.7
4	5~7 level	8.0~17.1
5	7~8 level	13.9~20.7

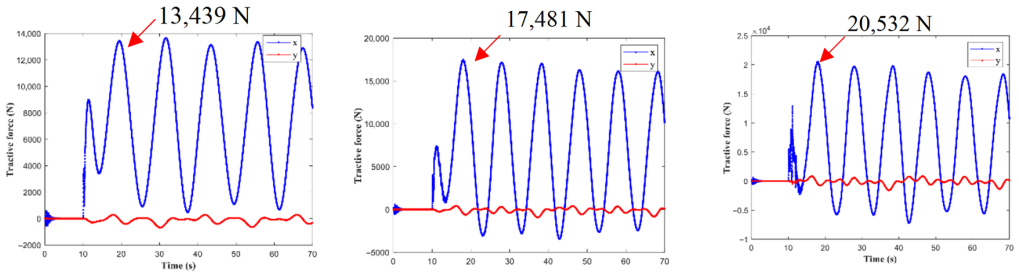
Since a level 1 sea state has less impact on the kinetics of a carrier plane, this study focuses exclusively on level 2–4 sea states that significantly affect traction safety. The wind speeds are set at 4 m/s for level 2, 8 m/s for level 3, and 13 m/s for level 4 sea states. The vertical area of the aircraft subjected to wind load is 32.04 m^2, and the vertical area of the tractor subjected to wind load is 1.4 m^2; the velocity of the tractor is 3.6 km/h. Figure 7 is time-varying Euler angles (roll angle) of aircraft and tractor in the z-axis under different sea states. Figure 7 illustrates the time histories of the roll (z-axis Euler) angles

of the aircraft and tractor centroids under different sea state levels. As the sea state level increases from 2 to 4, the roll motion amplitude of both the aircraft and the tractor increases significantly, indicating a stronger influence of wave-induced ship motions. The close similarity between the aircraft and tractor responses suggests that the coupled towing configuration effectively transmits hull motions through the tire–deck contact and tow bar connection. These results demonstrate that roll motion is a primary source of dynamic excitation for the towing system under high sea states. Figure 7 shows that the roll-angle swing grows as sea state worsens. Figure 8 presents the time-varying longitudinal and lateral traction forces of the tow bar under different sea state levels. With increasing sea severity, the fluctuation amplitude of the longitudinal traction force increases noticeably, while the mean force level remains relatively stable. In contrast, the lateral traction force exhibits irregular oscillations driven by roll and pitch motions of the ship. These results indicate that higher sea states intensify dynamic load transfer within the tow bar, which may accelerate fatigue damage and reduce towing safety.



(**a**) Aircraft (**b**) Tractor

Figure 7. Time histories of roll (*z*-axis Euler) angles of the aircraft and tractor centroids under different sea state levels (sea states 2–4), with a constant traction speed of 3.6 km/h and wind speeds corresponding to each sea state.

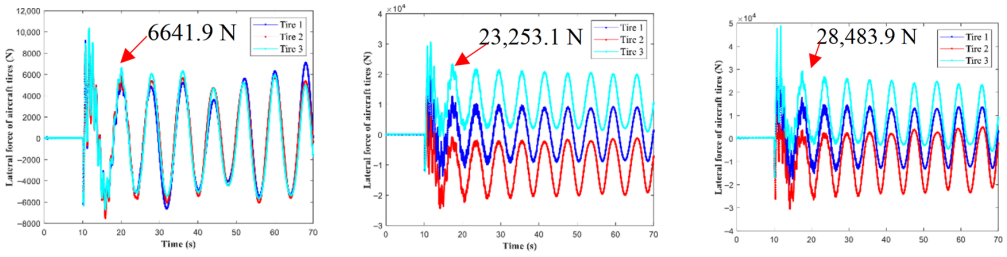


(**a**) Sea state 2 (**b**) Sea state 3 (**c**) Sea state 4

Figure 8. Time-varying longitudinal (*x*-direction) and lateral (*y*-direction) traction forces of the tow bar under different sea state levels (sea states 2–4), illustrating the influence of wave-induced ship motions on towing force fluctuations.

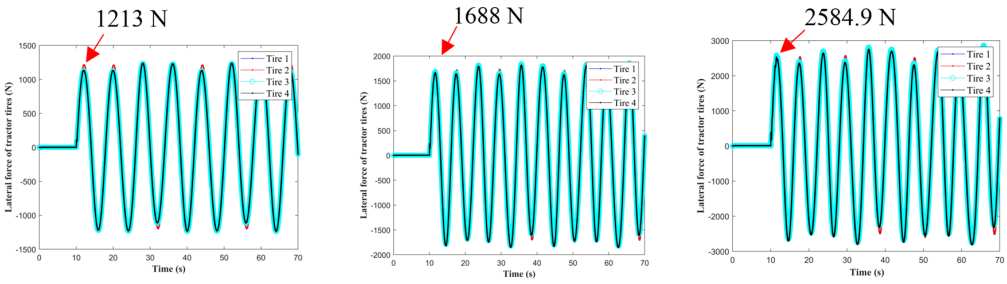
The lateral forces of aircraft and tractor tires are important parameters to judge the stability of traction system. Excessive lateral force causes huge lateral deformation of the tire, which may exceed the bearing range of tire and seriously affect the safety of aircraft traction system. The lateral forces of the aircraft and the tractor tires under the second, third, and fourth-level sea states are shown in Figures 9 and 10, respectively. Figure 9 shows the lateral force responses of the aircraft tires under sea states 2–4. Under sea state 2, the lateral forces of all tires remain relatively small and exhibit similar fluctuation patterns. As the sea

state increases to level 3, the lateral forces of the main landing gear tires increase sharply, indicating uneven load redistribution caused by coupled roll and heave motions. Under sea state 4, the lateral tire forces further increase and display intermittent sharp peaks, which are associated with transient off-ground and re-contact phenomena. This behavior significantly increases the risk of tire sideslip and loss of traction stability. From Figure 9a, it can be seen that after driving stability, the lateral forces of each aircraft tire under the second-level sea state show similar fluctuations, with a maximum value of 6641.9 N in the steady stage. The time-varying curve of lateral tire force under the third-level sea state is shown in Figure 9b. It can be seen that the fluctuation range of lateral force for each tire is different. The absolute value of lateral force for tire 2 and tire 3 is relatively larger than that of tire 1, and the fluctuation peak of tire 3 under the level 3 sea state in the stable stage is 23,253.1 N, which is 250.1% higher than that of the second-level sea state. Figure 9c shows the lateral force curve of the aircraft tire under the fourth-level sea state. Compared with the third-level sea state, the steady-state tire force under the fourth-level sea state increases by 22.5%. Figure 10 illustrates the lateral force responses of the tractor tires under different sea state levels. Similarly to the aircraft tires, the tractor tire lateral forces increase in magnitude as the sea state becomes more severe. However, the fluctuation patterns remain relatively consistent among different tires, indicating that the tractor experiences more uniform load distribution due to its lower center of gravity and shorter wheelbase. Nevertheless, the increasing force amplitude under higher sea states suggests a growing risk of reduced steering stability during towing operations. As the sea state level increases from level 2 to level 4, the amplitude of the force increases by 39.2% and 53.1%, respectively, and the change trend of each tire force remains unchanged. In summary, with the increase in sea state level, the lateral force of aircraft tire increases in multiples, the risk of aircraft tire sideslip increases sharply, and the safety and stability of the traction system decrease suddenly. In engineering practice, when the aircraft is transported under high sea states, the lateral force and sideslip risk of the aircraft tire should be focused on to ensure the safety of the aircraft traction.



(**a**) Sea state 2 (**b**) Sea state 3 (**c**) Sea state 4

Figure 9. Time histories of lateral forces acting on the aircraft tires under different sea state levels (sea states 2–4). Tires 1–3 correspond to the nose landing gear and the two main landing gears, respectively.

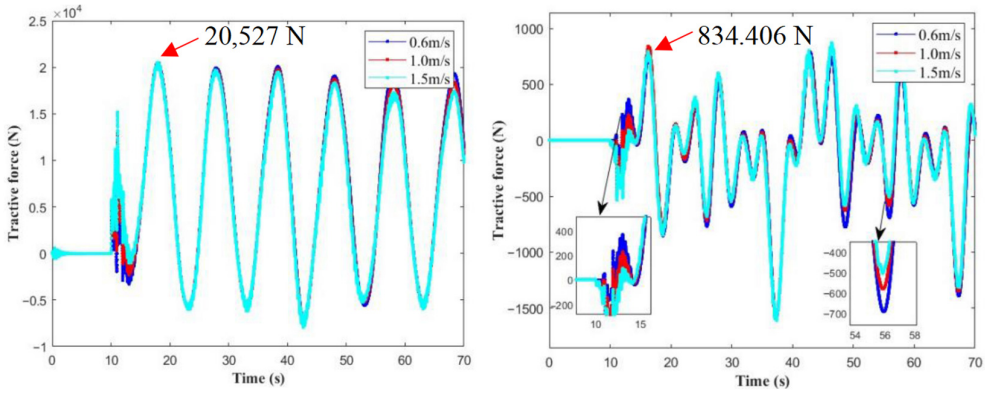


(**a**) Sea state 2 (**b**) Sea state 3 (**c**) Sea state 4

Figure 10. Time histories of lateral forces acting on the tractor tires under different sea state levels (sea states 2–4), showing the increase in force amplitude with increasing sea state.

4.4. Influence of Traction Speed on the Dynamic Characteristics of System Under High Sea States

Traction speed is one of the important parameters affecting the stability of the traction system of ship-borne aircraft. In high sea states, appropriate traction speed is a reliable way to improve the stability of the system. Therefore, the dynamic characteristics of the traction system at different speeds are studied in this section. Under the four-level sea states, the dynamic analyses are carried out at the traction speed of 0.6 m/s, 1 m/s, and 1.5 m/s, respectively, and the time-varying curves of longitudinal traction force are drawn, as shown in Figure 11a. It can be known that with the increase in traction speed, the longitudinal traction force is becoming larger in the initial stage. This is because the acceleration required to accelerate to the set speed in the same time is different, which leads to different force values, and the amplitude of the force gradually decreases in the uniform driving stage. Figure 11b is the lateral traction force at different traction speeds. It can be seen from the diagram that the amplitude of the traction force decreases with the increase in the traction speed in the uniform driving stage. It can be seen from the above that for the rod-traction system, when driving in a straight line under high sea states, the amplitude of the traction force decreases with the increase in the traction speed.



(**a**) (**b**)

Figure 11. Time-varying (**a**) longitudinal and (**b**) lateral traction forces under different traction speeds (0.6 m/s, 1.0 m/s, and 1.5 m/s) at sea state 4, illustrating the effect of traction speed on system dynamic response. (**a**) Time-varying curve of longitudinal (x-direction) traction force at different traction speeds. (**b**) Time-varying curve of lateral (y-direction) traction force at different traction speeds.

5. Discussion

The results of this study highlight the significant impact of ship motion on the dynamic behavior of ship-borne aircraft towing systems. By incorporating rolling, pitching, and heaving motions into multibody modeling, our analysis demonstrates that the coupled effects of ship motion play a decisive role in amplifying towing rod forces and tire lateral loads, directly affecting towing stability. This finding provides valuable quantitative insights into the towing process under complex sea conditions while also revealing limitations inherent in model simplifications. First, tire lateral force sensitivity increases markedly with rising sea state levels. Under sea state 3, lateral tire forces increased by 250.1%, indicating significant sea state influence on towing safety. This result aligns with prior studies, such as Zhu et al. [16], who observed similar trends in analogous vessel towing dynamics analysis, noting that worsening sea states cause severe lateral force fluctuations, thereby increasing the risk of towing instability. However, unlike Zhu et al. [16]'s study, our research further reveals that under sea state 4, the increase in tire force is accompanied by intermittent ground loss, posing greater challenges to the safety of the vessel towing system. This new finding highlights the profound impact of high sea states on towing stability and

tire lifespan, particularly as sea conditions worsen, significantly increasing the risk of tire skidding. Second, variations in traction speed exert a certain influence on the system's dynamic response. Results indicate that appropriately increasing traction speed can reduce lateral force fluctuations, thereby enhancing system stability to some extent. Although higher traction speeds increase traction demands during acceleration phases, lateral force amplitudes decrease significantly during steady-speed operation. This finding aligns with studies by Yang et al. [5] and Wang et al. [22] on the influence of traction speed on system stability, who also observed that higher speeds can mitigate dynamic disturbances caused by sea conditions. However, this study further highlights a noteworthy point: while increased traction speed reduces lateral force fluctuations, it may induce more dynamic coupling effects under complex towing conditions (e.g., during steering or braking maneuvers). Therefore, optimizing traction speed requires not only stability considerations but also comprehensive analysis tailored to specific operational conditions. Although our simulation study has revealed the dynamic response of the towing system under various sea states, the simplification of the model remains a significant limitation. First, this study assumes that the vessel's motion follows simplified harmonic motion, which overlooks the impact of irregular waves and sea state variations on the towing system. In reality, vessel motion is influenced by complex wave patterns that may exhibit nonlinear and stochastic characteristics, thereby exerting more intricate effects on the towing system. Compared to the work of Fricke et al. [7], which accounts for multiple wave patterns in vessel motion and proposes a more flexible model, our approach is less comprehensive. Therefore, future research should consider incorporating irregular wave models to more accurately describe the impact of actual sea conditions on the towing system. Additionally, the towing rod, aircraft, and tractor are assumed to be rigid bodies in this study. This assumption neglects structural flexibility effects, particularly the nonlinear behavior of the towing rod and landing gear. This simplification may underestimate the dynamic response of the towing system under high sea conditions, especially during complex mechanical interactions. Yang et al. [24] proposed that modeling the towing system as a flexible body better reflects structural responses under high sea states. Consequently, future work should consider incorporating flexible body models to further enhance simulation accuracy. It is worth noting that although we have not conducted large-scale physical validation, our model exhibits reasonable physical trends when compared with parameters and results from the existing literature. For instance, the increasing trends of traction force and tire lateral force with worsening sea conditions align with previous research findings (Li et al. [4], indicating that our model captures the primary dynamic mechanisms during the towing process. Future studies should consider experimental validation to further enhance the model's reliability and practicality.

Overall, this study provides a new quantitative analytical framework for carrier-based aircraft towing operations in complex sea conditions, revealing the profound impact of ship motion on towing stability and safety. However, limitations such as the simplified ship motion model and rigid-body assumptions require further refinement in future work. Future research may consider incorporating more complex wave models and nonlinear responses to better simulate the dynamics of towing systems in real-world environments. Through these enhancements, our model will be able to provide more precise safety guidance for carrier-based aircraft towing operations and offer a theoretical basis for optimizing traction speeds and system design in practical applications.

6. Conclusions

This study investigated the dynamic characteristics of a ship-borne aircraft rod-traction system under high sea states by establishing a coupled multibody dynamics model that

incorporates ship roll, pitch, and heave motions. The results demonstrate that sea state severity plays a dominant role in towing stability. As the sea state increases, both traction rod forces and tire lateral forces are significantly amplified. In particular, noticeable tire sideslip occurs at sea state 3, where the peak lateral tire force increases by approximately 250% compared with sea state 2, while intermittent off-ground phenomena and a further force increase are observed at sea state 4. These findings indicate that wave-induced ship motions can rapidly degrade towing stability and impose critical operational limits under rough sea conditions.

The influence of traction speed was also examined under high sea states. The results show that, although higher traction speeds lead to increased traction demand during the acceleration phase, the lateral force fluctuations during steady straight-line towing are reduced as speed increases. This suggests that appropriate traction speed selection can partially mitigate motion-induced disturbances and improve system stability under severe sea conditions. Overall, the proposed modeling framework provides quantitative insights into the coupled aircraft–tow rod–tractor–ship dynamics and offers practical guidance for assessing towing safety and operational limits of ship-borne aircraft in high sea states.

Despite the valuable insights provided by this study, there are several limitations. First, the current analysis focuses on straight-line towing operations with simplified harmonic ship motions, while more complex scenarios such as turning, braking, and combined longitudinal–lateral towing are not considered. These conditions could introduce additional dynamic coupling effects that may further influence towing stability. Second, the ship motion model used in this study does not fully capture the stochastic and irregular characteristics of real ocean waves under severe sea states. Additionally, the aircraft, tractor, and tow bar are modeled as rigid bodies, neglecting structural flexibility and nonlinear effects in the tow bar and landing gear.

Future work will extend the current framework to include maneuvering towing operations and irregular wave-induced ship motions. The incorporation of flexible body modeling, nonlinear tire–deck interaction, and advanced control strategies is expected to improve model fidelity. Experimental validation through scaled tests or hardware-in-the-loop simulations will also be pursued to enhance the reliability and practical applicability of the proposed approach.

Author Contributions: Conceptualization, G.N. and C.Z.; methodology, B.Z.; software, C.Z. and B.Z.; validation, G.N.; formal analysis, G.N.; investigation, B.Z.; resources, G.N.; data curation, S.Y.; writing—original draft preparation, B.Z.; writing—review and editing, C.Z.; visualization, J.H.; supervision, G.N.; project administration, G.N.; funding acquisition, G.N. All authors have read and agreed to the published version of the manuscript.

Funding: This project is supported by National Natural Science Foundation of China (Grant No. 52275118).

Data Availability Statement: The datasets analyzed during the current study are not publicly available, due to data being derived from a project, but are available from the corresponding author on reasonable request.

Conflicts of Interest: The authors declare that they have no known competing financial interests or personal relationships that could have appeared to influence the work reported in this paper.

References

1. Wang, X.W.; Peng, H.J.; Liu, J.; Dong, X.Z.; Zhao, X.D.; Lu, C. Optional control based coordinated taxiing path planning and tracking for multiple carrier aircraft on flight deck. *Def. Technol.* **2022**, *18*, 238–245. [CrossRef]
2. Leveille, M.J. Development of a Spacial Dynamic Handling and Securing Model for Shipboard Helicopters. Master's Thesis, Carleton University, Ottawa, ON, Canada, 2013.

3. Vilchis, J.C.A.; Brogliato, B.; Dzul, A.; Lozano, R. Nonlinear modelling and control of helicopters. *Automatica* **2003**, *39*, 1583–1596. [CrossRef]
4. Li, Y.; Zhao, D.; Zhang, Z.; Liu, J. An IDRA approach for modeling helicopter based on Lagrange dynamics. *Appl. Math. Comput.* **2015**, *265*, 733–747. [CrossRef]
5. Yang, H.; Ni, T.; Wang, Z.; Wang, Z.; Zhao, D. Dynamic modeling and analysis of traction operation process for the shipboard helicopter. *Aerosp. Sci. Technol.* **2023**, *142*, 108661. [CrossRef]
6. Zhao, D.; Zhao, Y.; Li, Y. Modeling and simulation of tractor and aircraft multibody system. In Proceedings of the International Conference on Intelligent System and Applied Material, GSAM 2012, Taiyuan, China, 13–15 January 2012; pp. 640–644.
7. Fricke, H.; Schlosser, M.; Garcia, M.A.; Kaliske, M. Embedding aircraft system modeling to ATM safety assessment techniques: The runway excursion safety case for runway strips with reduced strength. *Transp. Res. Interdiscip. Perspect.* **2019**, *3*, 100026.
8. York, B.; Alaverdi, O. A physically representative aircraft landing gear model for real-time simulation. In Proceedings of the Flight Simulation Technologies Conference, San Diego, CA, USA, 29–31 July 1996; p. 3506.
9. Linn, D.R. Development and Validation of a Planar on-Deck Helicopter Manoeuvring Simulation. Master's Thesis, Carleton University, Ottawa, ON, Canada, 2004.
10. Linn, D.R.; Langlois, R.G. Development and experimental validation of a shipboard helicopter on-deck maneuvering simulation. *J. Aircr.* **2006**, *43*, 895–906. [CrossRef]
11. Cui, J.; Nie, H.; Zhang, M.; Liu, G.; Long, S. Design optimization on shock absorbing performance of carrier-based aircraft landing gear. *Jisuanji Fuzhu Gongcheng* **2011**, *20*, 88–93.
12. Lu, X.; Sun, Y.; Tang, J.; Zhang, W. Analysis of kinematic characteristics of vehicle-aircraft traction sliding system considering wheel deformation. *J. Beijing Univ. Aeronaut. Astronaut.* **2025**, *51*, 478–486.
13. Dooley, G.; Martin, J.E.; Buchholz, J.H.J.; Carrica, P.M. Ship airwakes in waves and motions and effects on helicopter operation. *Comput. Fluids* **2020**, *208*, 104627. [CrossRef]
14. Shukla, S.; Sinha, S.S.; Singh, S.N. Ship-helo coupled airwake aerodynamics: A comprehensive review. *Prog. Aerosp. Sci.* **2019**, *106*, 71–107. [CrossRef]
15. Memon, W.A.; Owen, I.; White, M.D. Motion fidelity requirements for helicopter-ship operations in maritime rotorcraft flight simulators. *J. Aircr.* **2019**, *56*, 2189–2209. [CrossRef]
16. Zhu, Y.; Lu, Y.; Sun, F.; Cheng, Q.; Wang, S.; Li, Z. Simulation Experiment Analysis and Verification of Ship Resonance for Shipboard Helicopter. *J. Phys. Conf. Ser.* **2021**, *2029*, 012015. [CrossRef]
17. Wen, Z.; Zhi, Z.; Qidan, Z.; Shiyue, X. Dynamics model of carrier-based aircraft landing gears landed on dynamic deck. *Chin. J. Aeronaut.* **2009**, *22*, 371–379. [CrossRef]
18. Yoo, B.W.; Park, K.P.; Oh, J. Dynamics simulation model for the analysis of aircraft movement characteristics on an aircraft carrier deck. *Int. J. Nav. Archit. Ocean. Eng.* **2024**, *16*, 100591. [CrossRef]
19. Liu, J.; Han, W.; Peng, H.; Wang, X. Trajectory planning and tracking control for towed carrier aircraft system. *Aerosp. Sci. Technol.* **2019**, *84*, 830–838. [CrossRef]
20. Zhang, Z.; Lin, S.L.; Zhu, Q.D. Genetic collision avoidance planning algorithm for irregular-shaped objects with kinematic constraints. *Acta Aeronaut. Astronaut. Sin.* **2015**, *36*, 1348–1358.
21. Li, K.; Li, X.; Wu, Y.; Deng, Z.; Wang, Y.; Meng, Y.; Li, B.; Su, X.; Wang, L.; Wang, X. Autonomous dispatch trajectory planning of carrier-based vehicles: An iterative safe dispatch corridor framework. *Def. Technol.* **2025**. [CrossRef]
22. Wang, Y.; Yu, H. Research on stability of carrier-based aircraft traction vehicle based on RBF neural network adaptive sliding mode control technology. *J. Ordnance Equip. Eng.* **2025**, *46*, 322–332.
23. Sun, J.; Yu, M.; Yang, D.; Tang, H.; Bian, D. Path planning of carrier aircraft traction system based on CL-RRT and MPC. *Syst. Eng. Electron.* **2024**, *46*, 1745–1755.
24. Yang, S.; Wang, K.; Zhang, B. Dynamic analysis of towing operations for shipborne aircraft under extreme sea conditions. *J. Ship Res.* **2021**, *62*, 219–228.

Disclaimer/Publisher's Note: The statements, opinions and data contained in all publications are solely those of the individual author(s) and contributor(s) and not of MDPI and/or the editor(s). MDPI and/or the editor(s) disclaim responsibility for any injury to people or property resulting from any ideas, methods, instructions or products referred to in the content.